Effects of Protein−Polyelectrolyte Affinity and Polyelectrolyte Molecular Weight on Dynamic Properties of Bovine Serum Albumin −Poly(diallyldimethylammonium chloride) Coacervates

ARTICLE *in* BIOMACROMOLECULES · MAY 2005

Impact Factor: 5.75 · DOI: 10.1021/bm049174p · Source: PubMed

5 AUTHORS, INCLUDING:

Himadri Bohidar
Jawaharlal Nehru University
185 PUBLICATIONS **1,921** CITATIONS
SEE PROFILE

Christophe Tribet
Ecole Normale Supérieure de Paris
84 PUBLICATIONS **2,604** CITATIONS
SEE PROFILE

Effects of Protein−Polyelectrolyte Affinity and Polyelectrolyte Molecular Weight on Dynamic Properties of Bovine Serum Albumin−Poly(diallyldimethylammonium chloride) Coacervates

H. Bohidar,[†] P. L. Dubin,*[,‡] P. R. Majhi,[‡,§] C. Tribet,[||] and W. Jaeger[⊥]

School of Physical Sciences, Jawaharlal Nehru University, New Delhi 110067, India, Department of Chemistry, Indiana−Purdue University, Indianapolis Indiana 46202, Laboratoire de Physico-Chimie des Polymeres, UMR CNRS 7615, ESPCI, Université Paris 6, 10 rue Vauquelin, 75231 Paris Cedex 05, France, and Fraunhofer Institute of Applied Polymer Research, D-14476 Potsdam-Golm, Germany

Received December 28, 2004; Revised Manuscript Received February 21, 2005

Bovine serum albumin (BSA) and poly(diallyldimethylammonium chloride) (PDADMAC) spontaneously form, over a range of ionic strength *I* and pH, dense fluids rich in both macroions. To study their nanostructure, these coacervates were prepared at low *I* and high pH (strong interaction) or at high *I* and lower pH (weaker interaction), with polymer MWs ranging from 90K to 700K, and then examined by dynamic light scattering (DLS) and rheology. DLS shows a dominant and surprisingly fast protein diffusional mode independent of polymer MW; accompanied by robust slow modes, slower by 1−2 orders of magnitude, which are also insensitive to MW and are present regardless of *I*, pH, and sample aging. High MW sensitivity was observed by rheology for the terminal time (order of milliseconds), which increased as well with the strength of polyelectrolyte−protein interaction. Viscoelastic behavior also indicated a tenuous network, solidlike at low strain but re-forming after breakage by shear. Two models, both of which have strengths and defects, are put forward: (I) macroion-rich domains dispersed in a continuum of macroion-poor domains near the percolation limit and (II) a semidilute solution of PDADMAC chains with interchain friction modulated by transient BSA−PDADMAC association.

Introduction

The pioneering work of Bungenberg de Jong[1] and others in the mid-twentieth century[2] produced a wealth of experimental data on coacervation, that is, spontaneous liquid−liquid phase separation occurring from solutions containing oppositely charged polyelectrolytes. Despite considerable efforts, a detailed molecular description of these intriguing dense, optically clear and highly viscous fluids was not possible for these early investigations. The two major problems confronted were the rather poorly characterized nature of the polyelectrolytes used (for example, gum arabic and gelatin) and the reliance on what would now be considered primitive methods of instrumental investigation. Since that time, coacervation has been extensively employed in microencapsulation,[3] but fundamental work in this area has been neglected,[4] despite the wealth of instrumental techniques now available for the study of nanoscale and colloidal systems. These methods open the way for investigations on a previously unexplored range of time and length scales.

Coacervation not only is exhibited by oppositely charged polyelectrolytes but also occurs when one component is a charged colloidal particle, for example, a protein,[5] micelle,[6] or dendrimer.[7] Coacervation does not appear to perturb the structure of the colloidal particle, inasmuch as complexation and coacervation with a polycation results in little or no change in a protein's helical content,[8] binding to ligands,[9] or pH titration curve,[10] and only a modest change in enzymatic activity.[11] Similarly, the absence of structural changes in micelles upon coacervation with a polycation is implied by the absence of any change in dye solubilization[12] and is also supported by cryo-TEM observations.[13] These observations lead to technologically intriguing applications of such coacervation phenomena in, for example, protein separations,[14] enzyme immobilization,[11] and immobilized detergency for environmental applications.[15] Despite these areas of potential development and accompanying fundamental questions, the coacervation of polyelectrolytes with oppositely charged colloids has not been much explored. The influence of polyelectrolyte:colloid stoichiometry critical conditions for coacervate formation in protein−polyelectrolyte and micelle−polyelectrolyte systems was reported.[5,16] Subsequent investigations on polyelectrolyte−micelle coacervation defined these "phase boundaries" in terms of stoichiometry, polyelectrolyte molecular weight, and micelle size and shape[16] and ionic strength and micelle surface charge density.[17] There were several general conclusions: (1)

* Corresponding author: e-mail dubin@chem.iupui.edu.
[†] Jawaharlal Nehru University.
[‡] Indiana−Purdue University.
[§] Present address: Department of Pharmaceutical Chemistry, University of California, San Francisco, CA.
[||] Université Paris.
[⊥] Fraunhofer Institute of Applied Polymer Research.

10.1021/bm049174p CCC: $30.25
Published on Web 03/26/2005

Coacervation is preceded by the formation of soluble polyelectrolyte−colloid complexes and aggregates thereof. (2) Coacervation occurs when the net charge of these complexes approaches zero, which is controlled by the charge per colloid particle and the number of colloid particles bound per polyelectrolyte chain, the latter depending on both colloid:polyelectrolyte stoichiometry and the intrinsic colloid−polyelectrolyte binding constant. (3) Coacervation is enhanced by increased size of either polyelectrolyte and colloid, as long as the colloid is smaller. While these studies provided a foundation for further work by defining the experimental conditions for coacervate formation, they did not at all address the question of the molecular organization of the coacervates or the associated issue of dynamics.

Polyelectrolyte−colloid coacervation arises from polyelectrolyte−colloid complexation; this in turn is electrostatically driven and is enhanced by an increase in the surface charge density of the colloid σ or the linear charge density of the polyelectrolyte, and diminished by an increase in ionic strength.[18] In the case of proteins, σ is controlled by the pH in a complex manner that reflects the protein's surface charge heterogeneity. Nevertheless, protein−polyelectrolyte coacervation resembles a true phase transition, occurring abruptly at a precise pH, definable to within 0.02 pH unit,[19] although this transition may be broadened by system polydispersity. The dependence of this "pH_ϕ" on ionic strength, stoichiometry, and temperature was investigated in detail for the system composed of bovine serum albumin (BSA), poly(diallyldimethylammonium chloride) (PDADMAC), and aqueous NaCl.[19] These studies defined the range of conditions under which coacervate forms and also indicated the predominance of electrostatic effects; hydrophobic interactions were apparently negligible. However, they did not yield any information on the internal structure of the coacervate and its dynamics. Such understanding is essential for applications requiring rapid protein diffusion (e.g., bioreactors) or for the control of slower reorganization in microencapsulation.

Nanostructure and protein mobility within protein−polyelectrolyte coacervates are subjects of interest for several reasons, particularly since enzyme activity is barely reduced when the protein is entirely contained in 0.5−5 μm coacervate droplets.[11] This observation means not only that protein structure is unperturbed but also that the effective diffusivity of protein in the coacervate droplet is unexpectedly large, given the high viscosity seen when these droplets form a uniform liquid phase upon centrifugation. A number of theoretical treatments have appeared to explain polyelectrolyte coacervation,[20,21] but none provide much detail about the microscopic organization of these fluids, and in any event their relevance to colloid−polyelectrolyte coacervation is questionable. Fortunately, a wide range of optical, hydrodynamic, and microscopic techniques are available to probe colloid−polyelectrolyte coacervates. In the present work, we explore the nature of BSA−PDADMAC coacervates on various length scales, using two complementary techniques, dynamic light scattering and rheology. To discriminate among possible models for coacervate microscopic organization, we particularly focus on the effect of polycation molecular weight and the influence of pH, ionic strength, and temperature. Three low molecular weight distribution PDADMAC samples[22] along with a broad MWD commercial sample[23] (Merquat 100) were used. In the case of the BSA/PDADMAC system, centrifugation of a coacervated mixture separates the protein- and polymer-rich coacervate from the more dilute phase as an optically clear fluid, and in this sense the coacervates studied here differ from the more heterogeneous gum arabic/whey protein systems recently reported on by de Kruif and co-workers,[24] which are in fact mixtures of the dilute and condensed fluids formed upon spontaneous phase coacervation.

Our goal here is then to propose and refine possible models for the internal structure of a protein−polyelectrolyte coacervate, using rheology and dynamic light scattering to monitor the changes on different length scales that accompany an increase in polyelectrolyte MW, or an increase in protein−polyelectrolyte interactions via manipulation of pH and ionic strength. Since the structure of coacervates may be unique and is not known a priori, we have attempted to avoid interpretation biased by conventional models that may have limited relevance. For this reason, we have organized the presentation in the following way. In the Results section, we present only what is self-evident without recourse to any model. The Discussion section subsequently interprets first light scattering and then rheology with reference to additional hypotheses about structure and organization. Finally, we put forward two specific models and contrast the ways in which each might be used to account for the results.

Experimental Section

Materials. Poly(diallyldimethylammonium chloride) (PDADMAC) samples of different molecular weights were prepared by free radical aqueous polymerization of diallydimethlyammonium chloride[22] and characterized after dialysis and lyophilization by membrane osmometry. A commercial sample of PDADMAC (nominal molecular weight of 2×10^5) was obtained as Merquat 100 from Calgon Corporation and dialyzed and freeze-dried. The latter PDADMAC sample shows much broader molecular weight distribution than the others.[23] Bovine serum albumin (BSA) was obtained from Roche (CAS 9048-46-8). NaCl, sodium acetate, and standard NaOH, HCl, and acetic acid solutions were from Fisher Scientific. Milli-Q water was used in all experiments.

Methods: Coacervate Preparation. BSA (6 g/L) and PDADMAC solutions (1.5 g/L) were prepared separately in 0.05−0.10 M NaCl solution and filtered (0.22 μm AcetatePlus, Osmonics Inc). The pH of each solution was adjusted to 4 (noninteracting conditions) with 0.1 N HCl so that initial mixing would be completely homogeneous. These two solutions were mixed (1:1) and adjusted to the desired pH by gradual addition of 0.1 N NaOH, beyond the point of initial coacervation, around pH 6 at this ionic strength.[19] Because the composition of coacervates is essentially fixed by boundaries of a phase transition, the ionic strength, pH, and coacervate concentrations of polymer and protein cannot be varied independently.[24] To focus on the influence of

Table 1. Coacervates Prepared and Their Compositions

sample	PDADMAC MW (M_w/M_n)	pH	I (M)	% H_2O	% BSA	% PDADMAC	viscosity (Pa·s) at 1 s^{-1}
A	219K (1.55)	7.5	0.05	–	–	–	0.32
B	219K (1.55)	8.5	0.10	–	–	–	0.23
C	219K (1.55)	8.5	0.05	–	–	–	0.78
D	90K (1.55)	9.0	0.05	73 ± 1	24 ± 0.7	3.9 ± 0.1	0.73
E	219K (1.55)	9.0	0.05	75 ± 1	20.5 ± 0.6	3.5 ± 0.1	1.3
F	700K (1.52)	9.0	0.05	76 ± 1	21 ± 0.6	3.4 ± 0.1	13.6
G	200K (5.0)	9.0	0.05	72 ± 1	24.4 ± 0.7	4.5 ± 0.1	0.94

polymer length and protein/polymer association strength (modulated by pH and ionic strength, I), a constant protein/polymer weight ratio of 5 was maintained in the starting mixture. After settling overnight the mixture was decanted, the top clear solution (supernatant) was discarded, and the bottom layer, which mainly contains coacervate, was centrifuged for 20 min at 4000 rpm. The yield of this optically clear (pale yellow) and viscous fluid was usually ca. 1% (v/v) of the original protein−polymer mixture. Coacervate samples were prepared from PDADMAC of various molecular weights at pH 7.5, 8.5, or 9.0 and $I = 0.05$ or 0.10 M (Table 1). Note that pH and I always refer to the conditions at which coacervation took place, not the actual ionic strengths and pHs of the coacervates, both of which are unknown.

Compositional Analysis of Coacervates. Water contents in the coacervates were determined by replicate dry weight analyses. BSA content was determined by UV analysis: coacervate was dissolved in acetic acid−sodium acetate buffer (pH = 4.0) 0.45 M in NaCl, and absorbance was measured at 278 nm (Agilent 8453A UV−visible spectrophotometer) relative to a calibration curve for BSA in the same solvent. Identical spectra in the presence and absence of PDADMAC indicated its negligible contribution to UV absorbance. PDADMAC content was determined by size-exclusion chromatography (SEC) on an apparatus composed of a NSI-33R Milton Roy minipump, a Rheodyne model 7010 injector with a 100 μL sample loop, a Gilson 112 UV−vis detector, and a Waters Associates−Millipore R401 differential refractometer (RI) detector. A Superose 6 column (Pharmacia) was connected between the injector and detectors. Coacervate was dissolved in pH 4.0 acetate/0.45 M NaCl mobile phase buffer and its PDADMAC content was determined by reference to a RI PDADMAC calibration curve. In some coacervate samples (D and G, Table 1) the RI peaks of PDADMAC and BSA overlapped, so coacervates were hydrolyzed with concentrated HNO_3 to remove the interfering effect of BSA prior to SEC.

Dynamic Light Scattering. DLS was carried out with (1) a Brookhaven BI-9000AT goniometer and digital autocorrelator (Holtsville, NY) employing a 488 nm 100 mW argon-ion laser; (2) a DynaPro-801 instrument (Protein Solutions Inc., Charlottesville, VA) equipped with a 30 mW solid-state 780 nm laser and an avalanche photodiode detector; and (3) an ALV-5000 multi-τ autocorrelator system employing a 3 W, 514.5 nm argon-ion laser (SP2020, Spectra Physics, CA). Measurements were usually carried out at 25 ± 1 °C and 90° scattering angle, with additional angle and temperature dependence studies. Diffusion coefficients, D, or relaxation times, τ, were obtained from the autocorrelation functions by use of NNLS[25] (nonnegatively constrained least squares), CONTIN,[26] REPES[27] (regularized positive exponential sum) or Williams−Watts[28] fitting procedures, applied to data from the Brookhaven, Protein Solutions, and ALV systems, respectively. The last-mentioned algorithm is a form of "bimodal" analysis

$$g_2(\tau) - 1 = B(A_1 \exp(-\tau/\tau_1)^{w1} + A_2 \exp(-\tau/\tau_2)^{w2} + A_3) \quad (1)$$

which forces all data into two modes. It is considered to be generally the most coercive, but its lower sensitivity to noise in the function of the fitted relaxation times made it more reliable as a means of comparing gross variations of either slow or fast relaxations.

Rheology. Rheological measurements were performed on a strain-controlled rheometer (Rheometrics Fluids spectrometer II, Rheometrics, Inc., Piscataway, NJ) fitted with cone−plate geometries (25 or 50 mm in diameter). Samples were slowly loaded onto the plate, and 10−15 min was allowed for the stresses to relax and for thermal equilibration (25 °C). The elastic modulus G' and the loss modulus G'' were obtained by subjecting samples to dynamic oscillatory tests during which a sinusoidal strain was applied and the resulting stress was recorded. From strain sweep tests, the linear viscoelastic region was determined to extend at least up to a a strain of 20%. Frequency sweep experiments were performed at a low amplitude of strain (<10%), covering the range 0.01−100 rad/s. At lower frequencies, the time required for measurements was long, and difficulties arose due to evaporation or condensation. Characterization of each sample was completed at different temperatures (in the range 1−35 °C), beginning at low T. After the last incubation at 35 °C, recovery of initial behavior was checked by cooling back to 25 °C.

Results

Compositional Analysis. As shown in Table 1, compositions were determined for samples D−G, all prepared at pH 9 and $I = 0.05$ M, with polymer MW ranging from 90K to 700K. The polymer concentration within the coacervate is seen to be independent of MW, but the observed viscosity increased strongly with polymer MW; this is clearly not attributable to a decrease in water content. The observed macroscopic viscosity of the coacervates increased strongly with PDADMAC MW at fixed I (0.05 M) and pH (9.00) (samples D−G) and, at fixed polymer MW, with increase

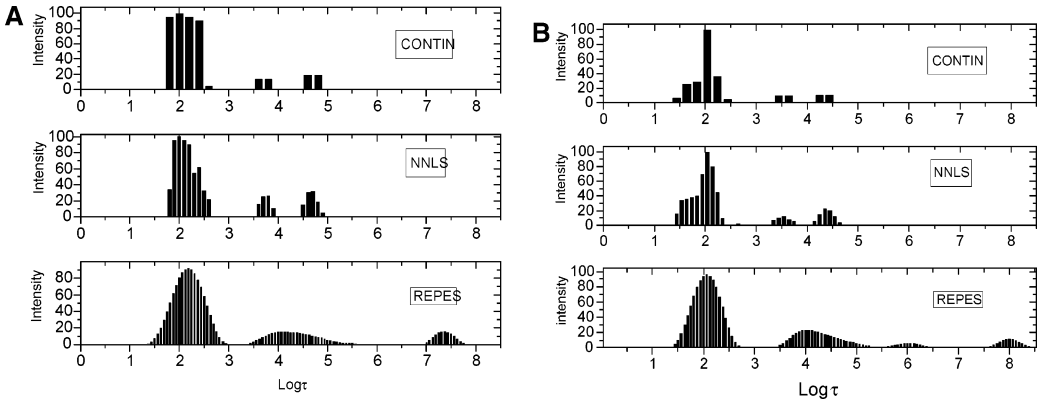

Figure 1. (A) Relative intensity vs log τ (τ is in microseconds) for sample E (MW 219K, pH 9.0, $I = 0.05$), showing the consequences of different fitting procedures. (B) Sample D (MW 90K, pH 9.0, and $I = 0.05$).

in pH (samples C and E) or decrease in I (samples B and C). As will be discussed below, the last two effects are related to an increase in the magnitude of polyelectrolyte−protein interaction energy. The sample prepared with commercial PDADMAC remains out of trend from the other coacervates prepared from narrow MW distribution PDADMAC.

Dynamic Light Scattering. DLS was carried out most typically at a 90° scattering angle and at 25 °C for coacervates, for BSA alone in 0.05 M NaCl at pH 6.5, and for PDADMAC alone in 0.05 M NaCl. All coacervate samples displayed at least two modes. It was important to confirm that these apparent distributions of diffusion coefficients were not artifacts of the deconvolution of the autocorrelation function or overly dependent on the means of sample preparation. In addition, we wished to settle upon one standard algorithm. The reliability of the various fitting procedures (CONTIN and NNLS for the BIC system, REPES and Williams−Watts for the ALV) was assessed by several criteria, primarily with the objective of maximizing robustness and consistency without loss of information. Robustness can be assessed in terms of (a) reproducibility of sequential analyses on a given data set, (b) repeatability from run to run on a given sample, and (c) reproducibility for a single sample over a period of time, the last also reflecting sample stability. Consistency here refers to the expectation of commonalities among results for samples that differ in minor ways, that is, the distributions of decay modes should not vary erratically. Finally, we reject methods such as cumulants,[29] which might satisfy the aforementioned requirements but clearly reduce the level of information accessible. Typical relaxation time (τ) vs intensity distribution curves are shown for samples E (219K, pH 9.0, 0.05 M) and D (90K, pH 9.0, 0.05 M), in Figure 1, panels A and B, respectively, in which Laplace inversion of the autocorrelation functions is accomplished by use of either CONTIN, NNLS, or REPES. All three fitting procedures were quite consistent with regard to the relative intensity and position of the fast mode, but only NNLS and CONTIN agreed on the position of the slow mode or modes (Figure 1). NNLS showed a uniform pattern of slow and fast modes among the various coacervate samples, and NNLS yielded the most reproducible distribution patterns for samples analyzed at different times after preparation, the sole exception being a diminution of the apparent diffusion coefficients for all modes after 4 months,

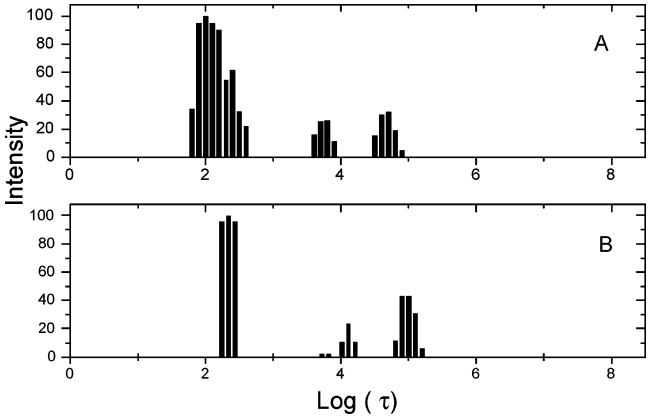

Figure 2. Relative intensity vs log τ for sample E (MW 219K, pH 9.0, $I = 0.05$), showing the reproducibility in distribution pattern: Lower curve is for a sample run 4 months after its initial run, shown in the upper curve.

likely due to sample dehydration (Figure 2). The mean diffusion coefficients for the fast mode are consistent from sample to sample in NNLS (see Figures 3 and 4) but the shapes of the fast mode are often variably asymmetric: Unlike REPES, NNLS makes little attempt to fit by use of continuous distributions. In any event, the exact peak width and shape for each component in a multimodal distribution cannot be reliable and such representations in fact correspond to overresolution. Therefore, we focus on the mean position and relative amount of the various modes, in regard to which NNLS results are quite consistent. The level of interpretation in later discussion takes into account the relative reliability of the different fitting procedures.

The NNLS distribution curves shown for all samples in Figures 3 and 4 display two or three diffusion modes: one fast mode, along with one or two slow modes which we designate as S1 and S2, respectively. The averages of the apparent diffusion coefficients associated with each mode are given in Table 2, along with viscosities, to facilitate later discussion. Samples D−G were also analyzed at different scattering angles (40°−120°), and the absence of angle dependence for the fast mode for the representative example of sample F, as shown in Figure 5, indicates its diffusive nature. The intensity of this fast mode scattering is always dominant, and the corresponding apparent diffusion coefficient ($\bar{D}^{\text{fast}}_{\text{app}}$) is on the order of $(1-2) \times 10^{-7}$ cm^2·s^{-1}, slower than the diffusivity of PDADMAC alone (2.4×10^{-7}

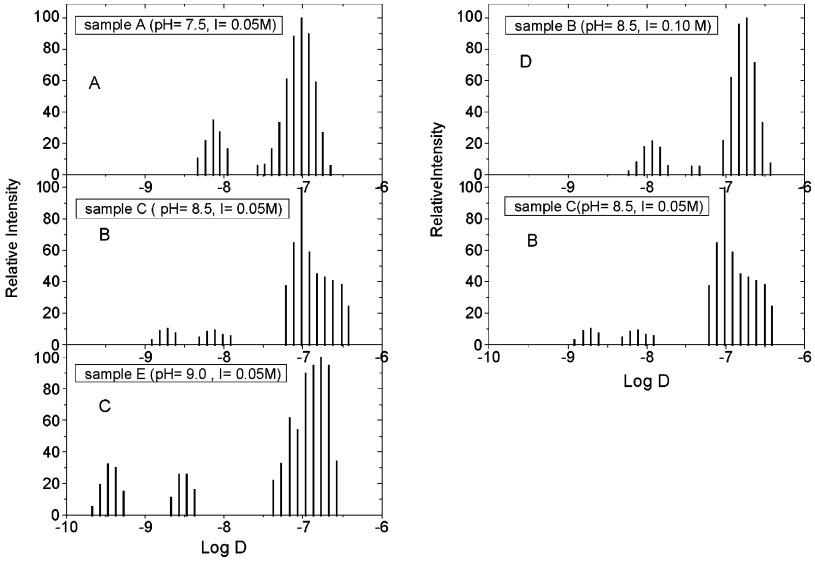

Figure 3. Relative intensity vs log *D* for coacervates prepared with BSA and PDADMAC (MW 219K) at constant ionic strength, $I = 0.05$ M, pH as shown (left) or at constant pH = 8.5 (right), ionic strengths as shown.

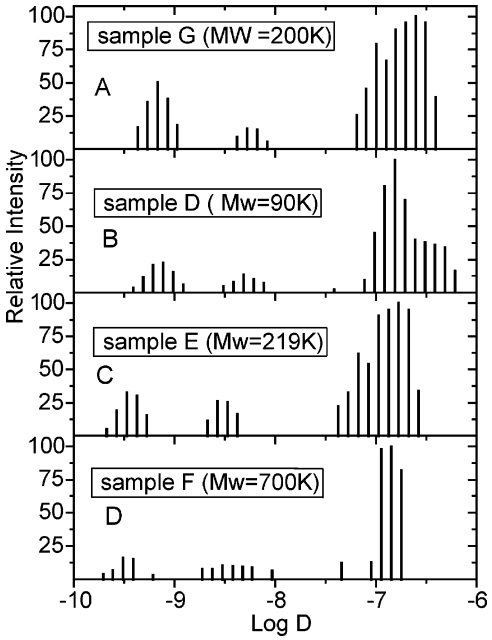

Figure 4. Relative intensity vs log *D* for BSA−PDADMAC coacervates prepared at pH = 9.00, $I = 0.05$ M, with polymers of different molecular weights, from top to botton: 200K, 90K, 219K, and 700K.

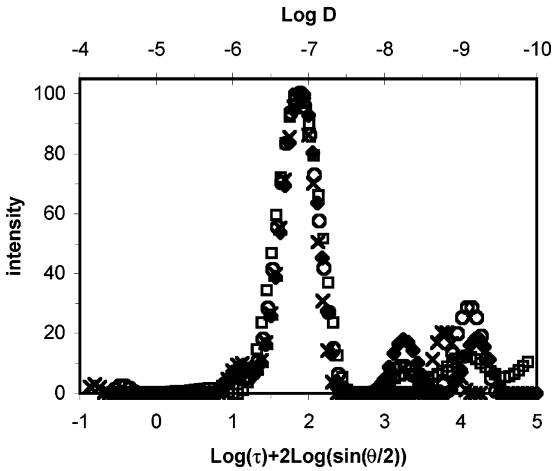

Figure 5. REPES analysis of DLS with sample F (MW 700K, pH = 9.0, $I = 0.05$ M) at different scattering angles. The distribution are shifted by 2 [log (sin (θ/2)] in order to superimpose the diffusive modes. The absence of superposition of slow modes is essentially due to noise. (◆) 120°; (□) 90°; (○) 60°; (×) 40°.

$cm^2 \cdot s^{-1}$, for 2×10^5 MW in 0.5 M NaCl) and about 3−4 times slower than the value for BSA alone, 7×10^{-7} $cm^2 \cdot s^{-1}$. Because the scattering intensity of BSA is much larger than that of PDADMAC because of its higher refractive index and concentration, it seems appropriate to attribute ($\bar{D}^{fast}_{app}$) to BSA. However, the apparent viscosity of the coacervate together with BSA coupling to the polymer would be expected to suppress the diffusivity of BSA by more than a factor of 3 or 4. Therefore, the unexpectedly large value of ($\bar{D}^{fast}_{app}$) is attributed to the motions of individual protein molecules rather loosely constrained by the polyelectrolyte system, that is, involving either the diffusion of unbound BSA or the motion of BSA coupled with an unentangled

Table 2. Observed Viscosity and Average Diffusion Coefficient Values of Various Coacervates

					$\bar{D}_{app} \times 10^7/cm^2\ s^{-1}$ (rel amplitude %)		
sample	polymer MW	pH	*I* (M)	viscosity (Pa·s) at 1 s^{-1}	S2	S1	fast
A	219K	7.5	0.05	0.32		0.07 (18)	0.9 (82)
B	219K	8.5	0.10	0.23		0.13 (15)	1.7 (85)
C	219K	8.5	0.05	0.78	0.018 (6)	0.08 (7)	1.3 (86)
D	90K	9.0	0.05	0.73	0.007 (13)	0.05 (8)	1.9 (79)
E	219K	9.0	0.05	1.3	0.004 (19)	0.03 (5)	1.2 (76)
F	700K	9.0	0.05	13.6	0.003(10)	0.04 (14)	1.4 (76)
G	200K	9.0	0.05	0.94	0.007 (19)	0.06 (5)	1.7 (76)

Table 3. Williams−Watts Parameters of the Correlation Functions Measured at a 90° Angle and 25 °C[a]

coacervate sample	log τ_1	log τ_2	w_2	intensity % of the fast mode
A	2.30 ± 0.01	3.09 ± 0.04	0.6 ± 0.1	61 ± 2
B[b]	2.3 ± 0.2	3.4 ± 1.1	0.5 ± 0.4	70 ± 30
C	2.21 ± 0.01	2.94 ± 0.03	0.8 ± 0.1	60 ± 2
D	2.03 ± 0.01	4.0 ± 0.1	0.41 ± 0.04	56 ± 4
E	2.16 ± 0.02	4.2 ± 0.2	0.30 ± 0.05	60 ± 4
F	2.12 ± 0.01	4.2 ± 0.2	0.30 ± 0.05	64 ± 4
G	1.95 ± 0.01	4.1 ± 0.2	0.35 ± 0.06	55 ± 2

[a] Least-squares fit with w_1 fixed at 1.0, B and A_3 fixed manually (eq 1); w_2 reflects the dispersity of the slow mode. Errors indicated are fitting errors for a single run but also were good approximation of the variance among separate runs. [b] For this sample, the slow mode was difficult to distinguish (having either too low an amplitude or being very close to the fast mode).

part of the PDADMAC. These alternate scenarios will be discussed later.

We define as "slow modes" those observed for all samples and with all instruments in the range of apparent diffusivities from 3×10^{-10} to 1.3×10^{-8} cm^2·s^{-1}. While these slow modes are not angle-dependent (Figure 5), their minor contribution compared to the fast mode made REPES analyses less reliable; more consistent behavior is obtained with NNLS (Figures 3 and 4). The apparent diffusion coefficient of the faster of these two slow modes, $\bar{D}^{S1}_{app}$, ranged from 8×10^{-8} to 19×10^{-8} cm^2·s^{-1}. This mode, as seen by comparison of panels D and B or D and C in Figure 3, shifted to smaller diffusivities with increase in pH or decrease in I, respectively, that is, conditions of stronger interaction. The second slow mode, $\bar{D}^{S2}_{app}$, varied from 3×10^{-10} to 18×10^{-10} cm^2·s^{-1}, and its contribution to scattering intensity also increased with increase in pH or decrease in I at constant MW (Figure 3). At fixed pH and I, $\bar{D}^{S2}_{app}$ decreased by only a factor of 2 with increasing MW (Figures 4). The effect of pH at fixed MW and I was more dramatic, $\bar{D}^{S2}_{app}$ increasing by nearly an order of magnitude with a change of 0.5 pH units (Figure 3, samples C and E).

The validity of these effects was checked by use of the Williams−Watts bimodal analysis (Table 3). After optimization of the four parameters w_1, τ_1, w_2, and τ_2, the fast mode $\tau_1$was found to be fairly monodisperse ($0.9 < w_1 < 1$), the difference between 0.9 and 1 not significant compared to experimental precision. To limit the number of parameters, the data were fitted with a sum of an exponential and a stretched exponential (i.e., $w_1 = 1.0$), a model often applied to polymer networks. The results for samples A−G show weak sensitivity of the fast mode to pH, I, and polymer MW, with a maximum difference of ca. 2× in the relaxation times τ_1. At fixed polymer MW, the fast mode is reliably faster in the pH 9.0 sample (E) compared to pH 7.5 (A) and 8.5 (C); and at fixed pH and I, it is affected by polymer MW (samples D, 90K, and E, 219K), although to a lesser extent than the effect of pH. With regard to the slow mode(s), the analysis in Table 3 suggests a less disperse mode at lower pH (samples A−C, $w_2 = 0.5-0.8$), although the determination of dispersity is less accurate at low pH (e.g., w_2 for sample B). The slow mode shows a significant increase in both dispersity (i.e., decrease of w_2 to <0.4) and average relaxation time τ_2 (by more than 10×) upon increasing pH to 9.0 (samples D−G). The influence of PDADMAC MW on τ_2, w_2, or w_1 was small compared to the uncertainty of the analysis.

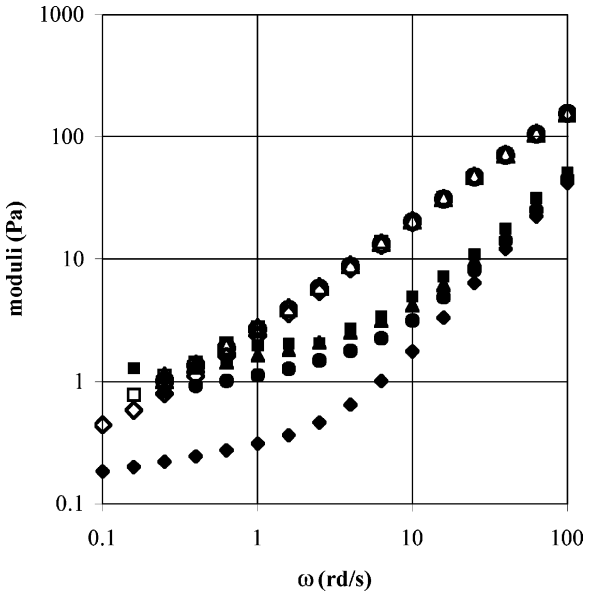

Figure 6. Apparent G' (solid symbols) and G'' (open symbols) of coacervate sample G (pH 9.0, 50 mM NaCl, PDADMAC MW 200K) as a function of frequency of oscillating strain. Measurements were performed at different amplitude of strain: (■, □) 1%, (▲, △) 10%, (●, ○) 20%, and (◇, ◆)100%. G'' remains unaffected by change in strain.

If the polyelectrolyte−protein interaction that drives coacervation is temperature-dependent, structural or dynamic changes in the coacervate could be reflected in alterations of diffusive modes with temperature. Therefore, DLS measurements were carried out from 4 to 35 °C. The apparent slow diffusion modes were again simplified by fitting the autocorrelation function to eq 1, in which the slow modes were treated as a single average mode. Because results obtained with samples D−G did not differ significantly, Table 4 shows only results for samples E (219K, pH = 9.0, I = 0.05 M) and G (200K, pH = 9.0, I = 0.05 M). The 2-fold decrease in fast mode relaxation times over the

Table 4. Log τ Values for Different Modes of Distribution Measured at Different Temperatures but Constant 90° Angle[a]

		temp/°C				
sample	mode	4	10	15	25	35
E	slow	4.75 ± 0.2	3.9 ± 0.2	−	4.2 ± 0.2	3.8 ± 0.2
	fast	2.33 ± 0.01	2.25 ± 0.01	−	2.16 ± 0.02	2.06 ± 0.01
G	slow	4.15 ± 0.15	−	3.9 ± 0.15	4.1 ± 0.2	4.0 ± 0.1
	fast	2.15 ± 0.01	−	2.03 ± 0.01	1.95 ± 0.01	1.85 ± 0.01

[a] Fitting conditions for Williams−Watts model were as described in Table 3.

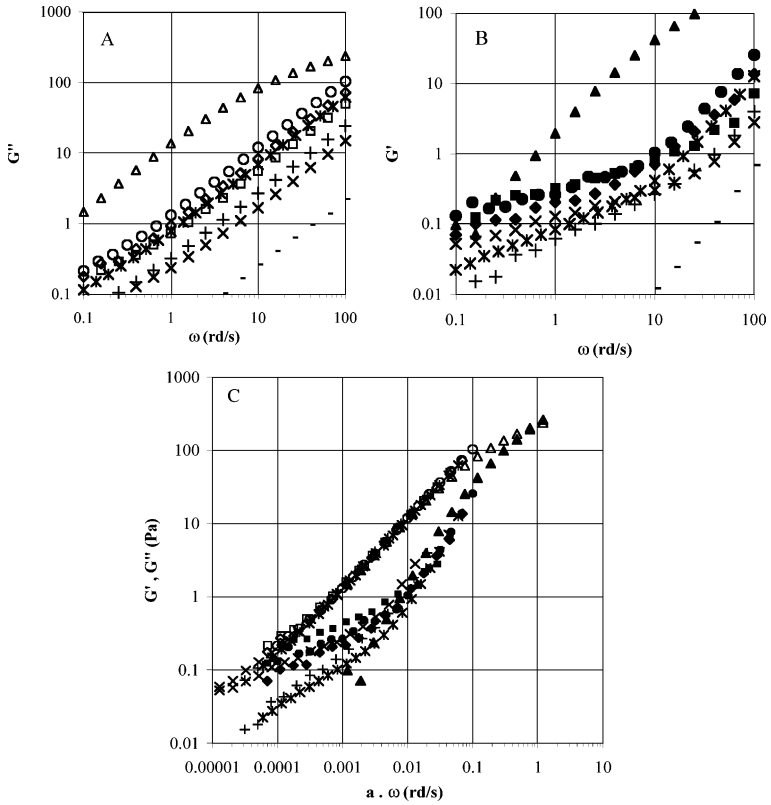

Figure 7. (A) Loss moduli G'' and (B) elastic moduli G' of coacervate samples or a PDADMAC solution at 25 °C as a function of the frequency of oscillation of strain. Amplitude of strain was 4% (any coacervates) or 100% (PDADMAC). Symbols stand for the coacervate A (+); B (×); C (*); D (□, ■); E (○, ●); F (△, ▲); G (◇, ◆); 3.5 wt % PDADMAC in 50 mM NaCl (-). (C) Storage and loss moduli versus reduced frequency in small amplitude oscillatory deformation (4%) for the coacervate samples at 25 °C. Same symbols as in panels A and B. Values of the shift factor *a* have been chosen to locate the crossover of the moduli at 1 as follows: A (2×10^{-4}), B (1.3×10^{-4}), C (6×10^{-4}), D (4.5×10^{-4}), E (10^{-3}), F (0.012), and G (7×10^{-4}).

temperature range is exactly consistent with the drop in the viscosity of water, confirming that it is a conventional diffusive mode. The larger uncertainty in the slow mode made it more difficult to establish viscosity as the only contributor. The absence of large variations (e.g., sample G) in the relaxation time, together with the absence of change in the relative scattering intensities of slow and fast modes (not shown), suggests the absence of dramatic changes in structure or aggregation state induced by temperature.

Rheology. To characterize the mechanical properties of coacervates, we measured frequency-dependent viscoelastic moduli with samples subjected to different strain amplitudes Γ. The results shown in Figure 6 for coacervate G are similar to those of coacervates E and D. Strain does not affect the moduli below 10%, and at 20% strain the results differ little from the results at low strain. In contrast, higher Γ obviously affects the measurements, especially at low frequencies, which make determination of G' and G'' unreliable beyond $\Gamma = 20\%$ strain. In samples D, E, and G, a pseudo-plateau value of G' is clearly present at low frequency but vanishes upon increasing Γ. In contrast, the coacervate sample prepared with the longest polymer chains (F) responds to Γ linearly up to 200% at all frequencies and exhibits no clear G' plateau at low frequency (not shown). $\Gamma = 4\%$ strain was therefore a good compromise, making it possible to obtain strain-independent moduli and providing high enough stress for accurate measurements down to 0.1 rad/s, even with the more fluid samples.

Table 5. Shear Modulus G_0 and Terminal Relaxation Time for Coacervates at 25 °C[a]

		sample						
	PDADMAC	A	B	C	D	E	F	G
G_0 (Pa)	9.5	150[b]	90[b]	350	400	450	300−430	450
τ (ms)	3.1	0.5[c]	0.4[c]	2.1	1.5	2.5	10	2.0

[a] Determined from interpolation of G' and G'' by use of the Maxwell model [b] Underestimated value, due to the lack of data at high enough frequencies. [c] Estimates obtained from the frequency shift factor used in Figure 2C. Error in G_0 is typically 50 Pa; error in τ is about 0.2 ms.

All samples show viscous character, with G'' larger than G' in the high-frequency range (Figure 7A,B). At fixed pH = 9.0 and $I = 0.05$ M, the moduli increase with PDADMAC MW; however, moduli of samples D, E, and G (90K < MW < 219K) differ by a factor of 3 or less, while sample F (700K) obviously exhibits markedly higher moduli (∼20× the moduli of D). A decrease in pH or an increase in I decreased moduli by an additional factor of ∼2, a result that would be consistent with the weakening of protein/polymer interaction under these conditions.[19] It is notable that significantly smaller moduli are obtained in the absence of protein, for example, the result for a 3.5% solution of 219K PDADMAC in 50 mM NaCl (Figure 7B).

In the absence of protein, that is, a 3.5% polymer solution in 50 mM NaCl, the frequency dependence of the moduli exhibited typical Maxwellian behavior. The corresponding relaxation time τ and the shear modulus G_0 were obtained by fitting the data to eq 2a,b (Table 5).

$$G'(\omega) = G_0\tau^2\omega^2/(1 + \tau^2\omega^2) \quad (2a)$$

$$G''(\omega) = G_0\tau\omega/(1 + \tau^2\omega^2) \quad (2b)$$

In the conventional view of entangled polymer solutions, G_0 varies in proportion to interchain contacts and τ varies in proportion to the slowest chain dynamics, that is, to the time required for relaxation of the chain conformation to equilibrium. To compare the protein-free PDADMAC solution with the coacervates in terms of degree of interchain contacts and chain dynamics, the values for a pseudo-rubbery plateau G_0 and the terminal time τ must be obtained for coacervates. To this end, the coacervate data were analyzed by two approaches: first, a fit with the simple Maxwell model in the appropriate (though limited) range of frequency; and second, the superposition of all the data on a master curve by use of frequency shifts. For all coacervates, the loss moduli G'' are proportional to ω (slopes of 1 in Figures 6 and 7A) and higher than G' in the high-frequency range, as expected for Maxwellian behavior at $\omega < 1/\tau$. The curves representing G' approach Maxwellian behavior asymptotically (at $\omega < 3$ rad/s for F) with average slope of about 1.5 (Figures 6 and 7B). This behavior reflects the contribution of a distribution of relaxation times in the experimental window. Nevertheless, we plotted $G'/\omega G''$ vs ω in the frequency window 1−100 rad/s. The curves show a pseudo-plateau that was used to estimate an apparent relaxation time, with the result shown in Table 5. Similarly, an apparent G_0 was calculated from the plateau value of $G''^2(1 + \tau^2\omega^2)/G'$ in the same limited frequency range. With an uncertainty of ±50, the values for samples C−F are not significantly different. G_0 remains between 350 and 450 Pa, including the case of the high MW sample F. This sample exhibits the highest dynamic moduli G' and G'' in the experimental range of frequency but has essentially the same shear modulus G_0 as all the others. Interestingly, the value of G_0 for the PDADMAC solution with no protein is significantly lower than G_0 for coacervate samples, indicating that interchain connectivity is significantly enhanced in the presence of proteins.

The similar rheological properties of all coacervates submitted to high-frequency oscillations is made more explicit in Figure 7C, upon rescaling of the dynamics of polymer chains. Although this procedure does not provide any estimate of G_0, a master curve emerges in the plot of the moduli as a function of $\alpha\omega$, with the factor $\alpha = 1/\omega c$ being the reciprocal of the crossover frequency between G' and G'' (Figure 7C). These shift factors thus provide relaxation times. The G'' values are reasonably well superimposed over the whole experimental window, and those of G' are superimposed in the high-frequency region. The differences in viscoelastic properties among coacervates are thus related to changes in chain dynamics rather than in chain network structure, consistent with the absence of significant differences in G_0 from the Maxwell analysis. This behavior suggests the absence of marked differences between coacervate samples in terms of structural features such as the entanglement density or the number of interpolymer associations.

Maxwell analysis and superposition on a master curve consistently indicate short relaxation times with values smaller than 80 ms. These reflect the high lability of interchain or intercomplex interactions in coacervates. Both relaxation times (τ in Table 5 and a in Figure 7C) vary in the following order: B ∼ A < D < C ∼ G < E ≪ F. At pH 9.0 and $I = 0.05$ mol/L, this list follows the order of PDADMAC MW (from lowest to highest); and, at fixed MW (219K) and $I = 0.05$ mol/L, the order corresponds to increasing pH (E > C > A). Protein−polymer interactions, however, induce a marked increase in PDADMAC connectivity, as seen from the difference between G_0 in the presence and absence of BSA. Coacervation cannot be depicted as a simple slowing down of interchain friction in the initial PDADMAC network—that is, a simple frequency shift with G_0 of about 10 Pa, as predicted in sticky reptation models.[30]

To establish how the flow properties are controlled by some activation energy, we performed experiments at varying temperature (1−35 °C) for samples D−G. We display results for sample F, which as noted above exhibits markedly higher moduli than other samples, and for sample E, which is representative of samples D and G as well. At first glance, moduli vs frequency curves in Figure 8A show relatively

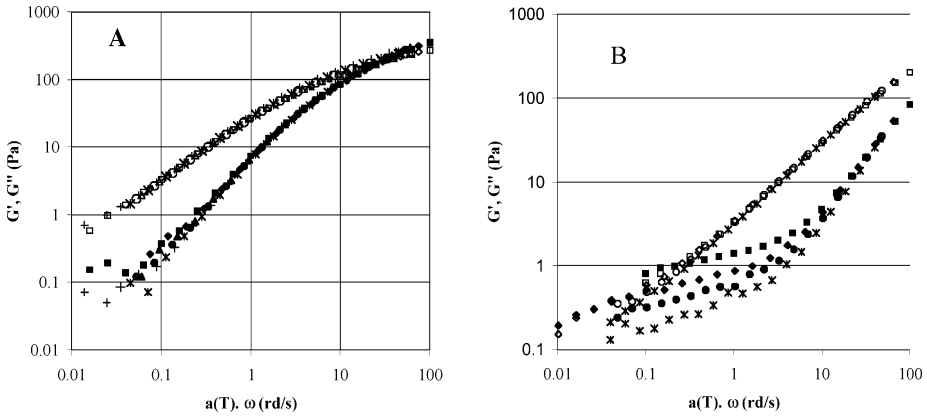

Figure 8. Storage (solid symbols) and loss (open symbols) moduli versus reduced frequency for coacervate samples at varying temperatures. The coefficient $a(T)$ is chosen to superimpose the data at high frequency. (A) Sample F (PDADMAC 700K, pH 9.0, 50 mM NaCl): values of $a(T)$ at 4°/10°/15°/20°/25°/35° = 1.0/0.75/0.60/0.53/0.45/0.35. (B) Sample E (PDADMAC 219K, pH 9.0, 50 mM NaCl): (■) 1 °C and $a = 1$; (◆) 9° and $a = 0.65$; (●) 18° and $a = 0.48$; (*) 25° and $a = 0.40$.

little temperature dependence. With sample F, excellent time−temperature superposition (TTS) is found by use of only horizontal shifts. Similarly, the whole range of G'' together with the high-frequency limit of G' enabled us to build TTS curves with all the other samples, by use of only frequency shifts (Figure 8B). Interestingly, the frequency shifts obtained this way were almost independent of sample; that is, shift factors in Figure 8 also apply to other samples. The increase in frequency by a factor of 3 over the temperature range used is of the order of magnitude of the decrease in viscosity of water over the same range. Because the dynamics follows the viscosity of the solvent, one may conclude that the major dissipation mechanisms are controlled by diffusion of chains in water, with no marked temperature dependence of interchain friction and association. This result supports previous calorimetric measurements showing that protein/polymer association is athermal[31] and complements the observation that pH_ϕ is temperature-independent.[19]

In contrast to the high-frequency behavior of G', the pseudo-plateau of G' at low frequency decreases consistently with increasing T. For all samples except F, attempts to shift data—either vertically or horizontally—failed to yield a master curve. While superposition is possible at high frequency (Figure 8B), or close to the crossover of G' and G''at low frequency, curves never superimpose over the whole experimental window. This reflects different and independent modifications of the structure and dynamics probed in high- and low-frequency ranges. Because the horizontal shifts used in Figure 8 normalize the curves by the water viscosity, and because G' has such a weak frequency dependence at low frequency and T, we considered that the TTS curves in Figure 8 allow for a comparison of the dependence of G' on T at low frequency (<10 rad/s). The value of G' in this range decreases by up to 10× upon increasing T. It does not depend on frequency (down to 0.01 rad/s), reflecting the storage of stress in a long lifetime network (>100 s). The tenuous nature of this network is indicated by the decrease in G' at strain higher than 20% (Figure 6). Its purely elastic contribution is indicated by the absence of significant modification of G'' when the plateau of G' decreases at high T, that is, when the network vanishes (Figure 8).

Discussion

The presence of several relaxation modes in DLS and the absence of time−temperature superposition in rheology both point to microscopic heterogeneity. Our goal is to interpret the results of both techniques in order to identify these heterogeneities. First, we discuss some conclusions that emerge from the results of each technique independent of model.

Dynamic Light Scattering. Since the scattering intensity of the polymer is so much weaker than that of the protein, the different modes in DLS must correspond to different spatial and temporal variations in protein concentration. We note that the typical length scale of heterogeneities must be smaller than the laser wavelength (514 nm) in order to be consistent with the transparency of the samples. As shown in Tables 2−4 and Figures 1−5, DLS measurements consistently show multiple decay modes with distributions of decay times that are (1) quite robust with respect to transform algorithms, (2) insensitive to polymer MW, and (3) only weakly dependent on scattering angle. The fast diffusion mode is most remarkably consistent, with respect to both its average value, $(1-2) \times 10^{-7}$ cm^2•s^{-1}, and its contribution to the total scattering (on the order of 70−80%). Because of its dominant contribution to the scattering intensity, and a diffusion coefficient less than 10× smaller than that of free protein [$(6-7) \times 10^{-7}$ cm^2•s^{-1}], it is difficult to imagine the fast mode arising from anything other than the diffusion of nonaggregated and surprisingly unrestricted BSA somewhere within the coacervate. The approximately 2-fold drop in $\bar{D}^{fast}_{app}$ with increase in temperature (Table 4), exactly consistent with the decrease in solvent viscosity, supports this hypothesis.

The slower mode, while less robust than $\bar{D}^{fast}_{app}$, is quite consistently resolved into two components, separated by about an order of magnitude in decay time for coacervates prepared at pH 9. While the location and relative scattering of these decays are, as mentioned, rather insensitive to most experimental variables, Table 2 shows that the slowest decay S2 makes a negligible contribution to scattering in samples A and B, this compensated for by an increase in the fast decay scattering. These samples, prepared at either lower pH or higher I, conditions of weakest protein−polycation interaction, also have the lowest viscosity. Sample C, as expected, represents an intermediate case, with the appearance of S2 but at a low level. The contribution to scattering of S2 is thus clearly correlated with the polyelectrolyte−protein interaction strength and its magnitude could be a measure of the number of proteins in regions of tight association.

Rheology. The apparent coexistence of regions showing "unrestricted" BSA motion with regions of tight association or aggregation of BSA leads to the question of their arrangement, in that either of those two could be the continuous phase in which the other is embedded. Rheology provides the best insight into this question, since viscoelastic properties reflect the connectivity or percolation of domains in heterogeneous materials. From the minor contribution of slow modes in DLS, it is expected that restricted domains constitute a small volume fraction of the coacervates. In addition, percolation of a tight interaction between dense domains is expected to result in an increase of elasticity. All samples show a dominant viscous nature, even at conditions of strong interaction (high pH and low I). The obvious sensitivity of the moduli G' and G'' to MW, pH, and I may reflect the growth of dense domains, but the samples never reached the critical point that characterizes the domination of flow properties by a long-lasting network.

An increase in either PDADMAC MW or the strength of the BSA−PDADMAC association (increased pH, decreased I) has little effect on the shear modulus G_0 but causes relaxation time (Table 5) and viscosity (Table 3) to increase by up to 20× and 60×, respectively. In fact, viscosity varies roughly in proportion to the relaxation time, which matches the conventional behavior of simple fluids, $\eta \sim G_0\tau$. The

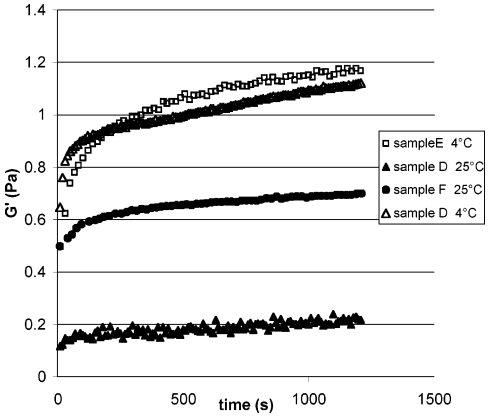

Figure 9. Elastic modulus G' as a function of time after preshearing. Samples were sheared at a shear rate of 10 s^{-1} for 1 min. At time 0, shear was stopped and dynamic moduli were measured every 10 s while maintaining an oscillating strain of 12% or 20% at a frequency of 0.5 or 0.7 rad/s (i.e., in the range of the pseudo plateau in G' as seen in Figure 7).

increase of viscosity with increasing pH is thus essentially ascribed to a slowing down of the self-diffusion of chains, arising from the tightening of the association with protein. Regardless of the composition of the continuous phase, it is reasonable to compare its behavior to the viscoelasticity of a semidilute polyelectrolyte solution, that is, vis-à-vis the expected flow properties of a concentrated solution of PDADMAC (maybe overlapped and sticky chains). In agreement with theory,[32] an increase in chain length at constant concentration markedly affects relaxation time but does not significantly change G_0. The predicted variation of terminal time τ with the square of polymer chain length even matches our data quantitatively (Table 5).[33] The behavior of sample G, between E and D despite its polymer MW similar to that of E, is likely due to its MW polydispersity.

The variation of moduli with frequency ω, especially the plateau value in G' at low ω, is, however, more complex than that predicted for entangled polymer solutions. It is possible to account for the elastic character (with G' eventually above G''at low T and low ω) assuming a solidlike tenuous network embedded into a viscoelastic suspending fluid, itself with pronounced viscous nature. Thus, at high ω, the suspending fluid dominates the mechanical properties, while the plateau modulus of the network appears at low ω. An unambiguous test of the validity of this picture comes from nonlinear behavior at conditions of strain that should break or at least strongly modify the tenuous network. Time-dependent measurements of the moduli at $\omega = 0.5$ rad/s were performed after extensive preshear, that is, 1−3 min at a shear rate between 1 and 100 s^{-1}. As expected, G' decreased markedly, by a factor of typically 2, a few seconds after the end of preshearing and then slowly recovered its initial value (Figure 9). This behavior did not depend on the conditions of preshearing or on the number of successive repetitions. Thus, the structure probed at low ω must be an equilibrium structure that forms upon slow organization of the viscous matrix. This behavior is reminiscent of the properties of mixed viscous fluid and weakly attractive carbon black particles as described by Trappe and Weitz.[32]

Two Proposed Models. The heterogeneities alluded to above will now be discussed in the framework of two possible models. Model I (Figure 10A) in the following refers to the presence of protein-rich domains leading to the formation of BSA-poor microphases as well. By definition, the microphases are significantly larger than both BSA and polymer chains. Model II, on the other hand, attributes the origin of both scattering and rheological properties primarily to a PDADMAC network with BSA connecting the polymer chains and considers the possibility of long-living clusters of chains and/or BSA as shown in Figure 10B.

According to model I, the process of coacervation begins when a transient localization of polymer segments produces an enhanced and uniform positive local potential domain, to which net negative proteins relocate; in so doing, they stabilize it. The interconnectivity of polymer segments leads to cooperativity and growth of such protein- and polymer-rich domains and thence to two homogeneous but not identical phases. Somewhat arbitrarily at this point, Figure 10A represents the discontinuous phase as the more dense of the two. Microscopically, the motion of protein depends on the rate of exchange and equilibration of polycations and BSA. This may resemble the proposed motions of proteins at proteoglycan-rich cell surfaces, in which proteins move freely from one polyanionic glycosaminoglycan to another, "like molecular Tarzans swinging from vine to vine".[35] A full description of model I would include the parameters required to interpret rheology and scattering data: (a) the volume fraction of the two phases, (b) the viscosity of the continuous phase, (c) the possibility of coalescence of the discontinuous phase, (d) the proximity to percolation, (e) the shape and dynamics of the interdomain boundaries, and (f) the relative refractive indices of the two domains. Clearly only a few of these features can be inferred from the present data.

Model II, in contrast to model I, preserves some of the original structure of the soluble protein−polyelectrolyte complex (PPC), that is, the coacervate precursor. Interchain contacts involving one BSA or clusters of BSA are presumed to provide cross-links having a long lifetime, which modulate the flow properties. The cartoon in Figure 10B is consistent with the known stoichiometry of the coacervate (BSA: PDADMAC = 20:3.5 w/w). A nonuniform distribution of protein along the polymer is shown with a typical size on the order of the distance between PPC overlaps (*Le*). Figure 10C is meant to indicate that the contact between protein and polymer may involve numerous polymer repeat units (here about 70) and to suggest that the trajectory of PDADMAC could be more extensive than portrayed in Figure 10B. As will be shown later, a reasonable value of the distance between inter-PPC cross-links *Le* is about 25 nm, that is, about 5 times the BSA radius. The broken circle represents the approximate dimensions of a single PPC. A full description of model II would include (a) the distance between inter-PPC overlaps, (b) the fraction of overlaps involving protein binding and acting as transient cross-links, (c) the fraction of protein bound, (d) the size and amount of BSA clusters, and (e) the lifetime of transient BSA−polymer association.

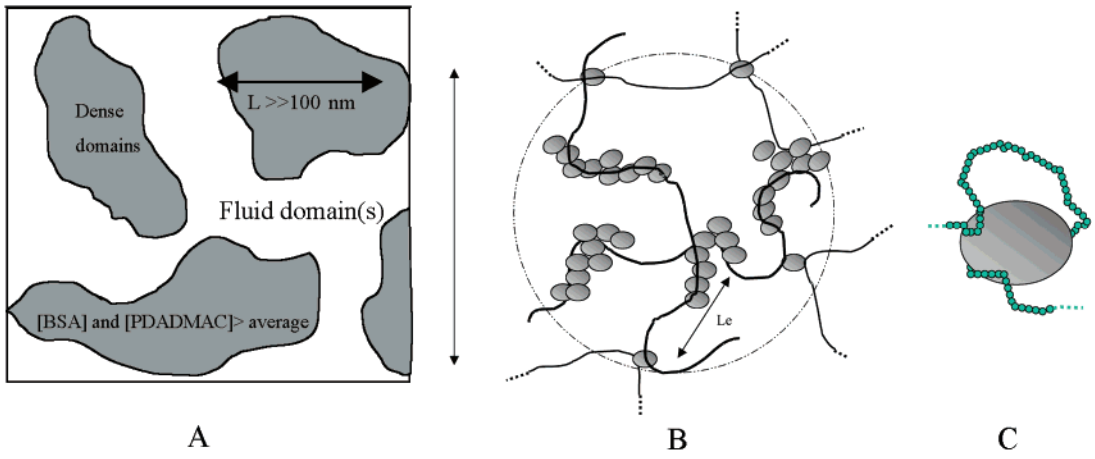

Figure 10. Models of coacervate structure: schematics of model I (A) and model II (B). (C) Zoomed picture of panel B.

Model I: (a) Dynamic Light Scattering. We now consider how DLS results refine model I. The relative amplitude of the fast mode and the essentially unrestricted motion of the protein are explained by the preservation of the majority of BSA within domains of low concentration of BSA, which are known to correspond to low macroscopic viscosity. Such rapid diffusion is likely to be partly responsible for the undiminished enzyme activity seen for coacervated enzymes.[11] The presence of dilute domains requires also domains with both viscosity and BSA concentration above the average, accounting for the slow modes S1 and S2. The remarkable fact that protein concentrations in excess of 20% (w/w) can maintain a fluid equilibrium and not undergo irreversible aggregation must be related to the polyelectrolyte network environment. It seems reasonable to attribute S2, with D_{app} on the order of 5×10^{-10} cm^2·s^{-1}, to motions within or fluctuations of such dense protein-rich domains. The high enzyme activity in coacervates indicates a dynamic equilibrium between protein-rich and protein-poor regions, and one may propose that events at these transient interfaces could account for S1.

(b) Rheology. Model I attributes the difference of viscosity (and relaxation time) between samples to the differences in size of highly viscous microdomains suspended in a fluid matrix. (The reverse case of a viscous matrix with dispersion of fluid domains cannot provide the protein fast mode because the rapid motion of BSA would be restricted in domains of size smaller than the laser wavelength.) The viscosity of colloidal dispersions in a solvent is with excellent approximation proportional to the solvent viscosity and a function of only one other parameter: the effective volume fraction of the dispersed objects. Several phenomenological expressions exist for this function, but all show weak η dependence on the volume fraction in dilute systems and a steep increase close to a critical effective fraction ϕ_c on the order of 64%, according to the Krieger−Dougherty equation:[33]

$$\eta = \eta_0(1 - \Phi_{eff}/\Phi_c)^m \qquad (m = -2) \tag{3}$$

The viscous domains in model I are presumed to have a viscosity 2 orders of magnitude higher than that of the dilute domains, because slow mode S2 is 2 orders of magnitude slower than the fast mode. The dominant fast mode in DLS corresponds to a fluid domain with viscosity typically $(3-5) \times 10^{-6}$ Pa·s, which contains the majority of the scattering species. Therefore, the observed viscosities in the range 0.23−13.6 Pa·s (Table 2) are consistent only with concentrated domains dispersed in the dilute phase, at an effective volume fraction Φ_{eff} above 60%. The shape of domains markedly affects the volume fraction Φ_{eff}, which for instance includes solvent trapped inside irregularly shaped domains. A value of Φ_{eff} close to Φ_c essentially means that a slight growth of the dispersed domains would result in strong interactions among them, possibly gelation of the sample, and the emergence of elasticity, which has not been observed.

The relative amount of the dense domains should correlate with the fraction of intensity attributed to the slow modes; however, the sum of the amplitudes of S1 and S2 is relatively constant, while the viscosity (and correspondingly the effective volume fraction of the domains) varies markedly. In the framework of model I, this lack of a simple relationship between scattering intensity and viscosity requires the assumption of dramatic differences in shape or roughness of the dense domains formed in different samples.

Model II. The features of model II are related to PPC chain overlap. First we assess the assumption of chains above the overlap concentration. With typical polymer concentrations of 35 g/L, the coacervates cannot be considered a dispersion of dilute chains, but the length scales corresponding to (a) the size of a single chain and (b) the correlation length, ξ, in the network of overlapped chains are not immediately evident. The reciprocal of intrinsic viscosity gives an estimate of the overlap concentration C^*, and the Mark−Houwink parameters for PDADMAC in 50 mM NaCl ($K = 2.4 \times 10^{-3}$ mL/g and $a = 0.975$)[33] lead to $C^* = 0.83$, 3, and 6.1 g/L for polymer MWs 700K, 200K, and 90K, respectively. However, measured viscosities vs polymer concentration for MW 219K lead to C^* of ca. 9 g/L at a viscosity of 0.002 Pa·s, this difference from calculated values probably due to MW polydispersity. An effective length R_e of the chains is calculated via

$$C^* \sim (\mathrm{MW}/N_a)R_e^{-3} \tag{4}$$

giving R_e =110, 50, and 30 nm for the 700K, 200K, and 90K polymers, respectively. This provides an order of magnitude estimation of the polymer radii. The variation of

the viscosity with polymer concentration up to 50 g/L matches the power law predicted for the semidilute unentangled regime[30] (data not shown). Clearly the polyelectrolyte matrix at 35 g/L with no protein is in the semidilute regime. The concentration dependence of ξ, which provides an estimate of the distance between interpolymer contacts, is thus predicted by use of the scaling law developed for polyelectrolytes in the low salt limit[30] (because 50 mM salt is small as compared to the concentration of monomer units): $\xi/R_e \sim (C/C^*)^{-0.5}$. For 219K polymers and a priori $R_e = 50$ nm, $C = 35$ g/L, and $C^* = 9$ g/L, we obtain for the corresponding distance between polymer chains $\xi_c = 24$ nm. Thus, for polymer alone (no proteins) at concentrations typical of the coacervate, the chains are above C^*, with a typical correlation length of ca. 25 nm.

Now we consider the entanglements of PPC chains in coacervates. In a network of transiently connected chains, the shear modulus G_0 is proportional to the concentration of inter-PPC bonds. The length of elastically active strands, *Le*, calculated from

$$G_0 \sim Le^{-3}kT \tag{5}$$

(k is the Boltzmann constant, and T is the temperature) is 21 nm, similar to the calculated correlation length in 35 g/L PDADMAC ($\xi \sim 25$ nm, see above). This suggests that the structure of polymer matrix is not markedly affected by association with BSA and implies that most interchain contacts are transiently frozen by association with BSA. Thus, the coacervates show mechanical properties similar to a matrix of 35 g/L overlapping PDADMAC chains, with interchain friction strongly correlated with the BSA/polymer association strength. The existence of a solidlike but fragile network revealed by rheology data points, however, to the presence of additional "clusters" in this matrix of entangled PPC, as shown in Figure 10B.

Model II can lead to fast and slow diffusive modes, but with protein motions strongly coupled with the motions of polymer chains. To the extent that the lifetime of BSA−polymer complexes is longer than the observed relaxation time, it is possible to predict a variety of protein dynamics arising from a variety of polymer segment dynamics at different length scales: BSA moves only by dragging along an associated polymer chain, and a slow motion is expected for diffusion of polymer−BSA complexes at length scales beyond the correlation length ξ of the PPC network. In contrast, rapid protein motion is coupled to the general breathing dynamics of the network involving cooperative fluctuation in the mesh size of the network. The fast mode corresponding to such dynamics obeys a form of Stokes law with *Le* in place of R_h. *Le* is about 3 times the BSA diameter, which is consistent with the apparent diffusion coefficient D_{app} associated with the fast mode being about 4 times smaller than the free solution D_{app} of BSA. With regard to the existence of two slow modes, the presence of clusters close to percolation as shown in Figure 10B provides a mode related to the motion of clusters, which add to the slow mode related to motion of PPC chains. To account for the observed S1 or S2, these clusters should not be trapped in the PPC network and thus cannot be much bigger than *Le*.

Conclusions

Rheology and DLS were used to probe the dynamics of protein−polyelectrolyte coacervates prepared at different pH and I, with BSA and PDADMAC with MWs from 90K to 700K. Both methods consistently showed contributions of rapid phenomena of diffusion and/or organization. A dominant DLS fast mode, independent of polymer MW, is ascribed to a protein fraction that, despite high macroscopic viscosity and the expected overlap of PDADMAC chains, is only loosely constrained. Rheology yields a terminal time on the order of milliseconds, highly sensitive to MW and typical of semidilute polymer solutions. Increasing the BSA−polymer interaction (by increased pH or decreased I) increases this terminal time, that is, slows down polymer chain motion, although only by an order of magnitude. The fast diffusion processes of both BSA and PDADMAC suggest fast exchange of proteins among binding loci on polymer chains. Both techniques showed additional phenomena with markedly slower dynamics, some at least 2−3 decades slower than the fast processes, detected as DLS slow modes or by the persistence of a low frequency elastic plateau modulus. DLS slow modes were remarkably robust and not strongly sensitive to pH, I, or sample aging, indicating an equilibrium between the continuous matrix of the coacervate and the frozen domains probed by DLS. Viscoelastic measurements reveal the formation of a tenuous network, solidlike at low strain. Reconstitution of this elastic character after breakage by extensive shear shows that this network must be formed at equilibrium. Thus, domains or percolated networks with "frozen" dynamics decorate the continuous (highly dynamic) coacervate matrix at equilibrium.

MW effects were expected to indicate the size of frozen domains relative to those of PDADMAC chains (~50 nm) and thus provide information about the microscopic origin of "frozen" dynamics. The large variation of viscoelasticity with MW, however, was probably dominated by the flow properties of the continuous matrix, with no obvious correlation to the emergence of the tenuous network. The slowest DLS mode was primarily sensitive to pH and I, making it difficult to quantify the apparently minor influence of MW.

All our results taken together, and including the effect of temperature, strongly constrain possible models of coacervate structure and dynamics; they may also suggest that no single model based on a single type of frozen domain or heterogeneity can encompass the full set of properties. For example, a semidilute matrix of polymer−protein complexes (model II) should be packed with a dispersion of small protein clusters (size < polymer size) close to percolation transition in order to account for elastic properties and DLS slow modes. But the persistence of the DLS mode at high temperature contradicts the obvious weakening of elastic properties ascribed to a partial disruption of the clusters. Alternatively, model I proposes a dispersion of microphases, large domains more dense in PDADMAC and BSA display-

ing markedly slower dynamics. The DLS slow modes are attributed to BSA diffusivity in these dense microphases and at their interface, while the DLS fast mode is attributed to a fluid continuum insensitive to either temperature or PDADMAC MW. Rheology then leads to the requirement of temperature- and MW-dependent dense microphase volume fractions in contradiction of DLS results. We note, however, that nothing excludes the coexistence of the types of heterogeneities described in the two models, nor the possibility of multiple chains entangling and exchanging free BSA molecules through constrained diffusion.

We conclude that both models capture some part of coacervate structure and dynamics. A dispersion of microphases (model I) explains the DLS slow modes. The complexity of flow is captured if the continuous matrix has the viscoelastic properties of a semidilute solution of PDADMAC chains with interchain friction modulated by transient BSA−PDADMAC association (model II). In addition, we propose the formation of a temperature-sensitive tenuous network that cannot be detected by light scattering. Coacervates are thus heterogeneous in many respects, a crucial feature being the existence of frozen domains suggested by both models, but neither type of heterogeneity is significantly affected by the size of PDADMAC. Tentative explanations of the absence of a MW effect are (a) formation of protein clusters significantly smaller than the smallest polymer chain used in this studies and (b) a significant contribution of counterion release to the formation and stability of dispersed microphase that compensates for the loss of polymer conformational entropy in phase separation.

Acknowledgment. We acknowledge support of NSF Grants DMR0076068 and CHE9987891 and PRF Grant 37190-AC7 (P.D.) and CNRS-NSF 10749 collaborative research grant (C.T. and P.D.). We thank Pierre Andrianjakamahefazafi for assistance in rheology measurements.

References and Notes

(1) (a) Bungenberg de Jong, H. G.; Kruyt, H. R. *Kolloid Z.* **1930**, *50*, 39. (b) Bungenberg de Jong, H. G. In *Colloid Science*; Kruyt, H. R., Ed.; Elsevier: Amsterdam, 1949; Vol. I.
(2) (a) Oparin, A. I.; Gladilin, K. L.; Kirpotin, D. B.; Chertibrim, G. V.; Orlovsky, A. F. *Dokl. Acad. Nauk. SSSR* **1977**, *232*, 485. (b) Oparin, A. I. *Origin of Life*; Dover Publications: New York, 1953.
(3) (a) Burgess, D. J.; Carless, J. *Int. Colloid. Sci.* **1984**, *98*, 1. (b) Burgess, D. J.; Singh, O. N. *J. Pharm. Phamacol.* **1993**, *45*, 586.
(4) Menger, F. M.; Sykes, B. M. *Langmuir* **1998**, *14*, 4131.
(5) Ahmed, L. S.; Xia, J.; Dubin, P. L.; Kokufuta, E. *J. Macromol. Sci.—Pure Appl. Chem.* **1994**, *A31*, 17.
(6) Dubin, P. L.; Davis, D. *Colloids Surf.* **1985**, *13*, 113.
(7) Leisner, D.; Imae, T. *J. Phys. Chem. B* **2003**, *107*, 8078.
(8) Mattison K. W. Ph.D. Thesis, Purdue University, West Lafayette, IN, 1999.
(9) Brouwer, M.; Cashon, R.; Bonaventura, J. *Biotechnol. Bioeng.* **1990**, *35*, 831.
(10) Wen, Y.-p.; Dubin, P. L. *Macromolecules* **1997**, *30*, 7856.
(11) Xia, J.; Mattison, K. W.; Romano, V..; Dubin, P. L.; Muhoberac, B. B. *Biopolymers* **1997**, *41*, 359.
(12) Sudbeck, E. A.; Dubin, P. L.; Curran, M. E.; Skelton, J. *J. Colloid Interface Sci.* **1991**, *142*, 512.
(13) Swanson-Vethamuthu, M.; Dubin, P. L.; Almgren, M.; Li, Y. *J. Colloid Interface Sci.* **1997**, *186*, 414.
(14) (a) Strege, M. A.; Dubin, P. L.; West, J. S.; Flinta, C. D. *Protein Purification: Molecular Mechanisms of Large-Scale Processes*; ACS Symposium Series 427; American Chemical Society: Washington, DC, 1990; pp 66−79. (b) Wang, Y.; Gao, J. Y.; Dubin, P. L. *Biotechnol. Prog.* **1996**, *12*, 356.
(15) Wang Y.; Banziger J.; Dubin P. L.; Filippelli G.; Nuraje N. *Environ. Sci. Technol.* **2001**, *35*, 2608.
(16) Li, Y.; Dubin, P. L.; Havel, H. A.; Edwards, S. L.; Dautzenberg, H. *Langmuir* **1995**, *11*, 2486.
(17) (a) Wang, Y.; Kimura, K.; Huang, Q.; Dubin, P. L.; Jaeger, W. *Macromolecules* **1999**, *32*, 7128. (b) Wang, Y.; Kimura, K.; Dubin, P. L.; Jaeger, W. *Macromolecules* **2000**, *33*, 3324.
(18) (a) Muthukumar, M. *J. Chem.. Phys.* **1987**, *86*, 7230. (b) Muthukumar, M. *J. Chem. Phys.* **1987**, *103*, 4723. (c) Evers, O. A.; Fleer, G. J.; Scheutjens, J. M. H. M.; Lyklema, J. *J. Colloid Interface Sci.* **1986**, *111*, 446. (d) Mattison, K. W.; Wang, Y.; Grymonpré, K.; Dubin, P. L. *Macromol. Symp.* **1999**, *140*, 53.
(19) Kaibara, K.; Okazaki, T.; Bohidar, H. B.; Dubin, P. L. *Biomacromolecules* **2000**, *1*, 100.
(20) Veis, A.; Border, E.; Mussell, S. S. *Biopolymers* **1967**, *5*, 37.
(21) Sato, H. Nakajima, *Colloid Polym. Sci.* **1974**, *252*, 944. (b) Tainaka, K. *Biopolymers 1980*, *19*, 1289.
(22) Dautzenberg, H.; Görnitz, E.; Jaeger, W. *Macromol. Chem. Phys.* **1998**, *199*, 1561.
(23) Dubin, P. L.; Levy, I. *J. Chromatogr.* **1982**, *235*, 377.
(24) (a) Weinbreck, F.; Tromp, R. H.; de Kruif, C. G.; *Biomacromolecules* **2004**, *5*, 1437−1445. (b) Weinbreck, F.; Rollema, H. S.; Tromp, R. H.; de Kruif, C. G. *Langmuir* **2004**, *20*, 6389−6395.
(25) (a) Lawson, C. L.; Hanson, R. J. *Solving Least Squares Problems*; Prentice Hall Inc.: Englewood Cliffs, NJ, 1974. (b) Morison I. D.; Grabowski, E. F.; Herb, C. A. *Langmuir* **1985**, *1*, 496.
(26) Provencher, S. W. *Comput. Phys. Commun.* **1982**, *27*, 229.
(27) Jakes, J. *Collect. Czech. Chem. Commun.* **1995**, *60*, 1781
(28) Stepanek, P. In *Dynamic Light Scattering: the method and some applications*; Brown, W., Ed.; Clarendon Press: Oxford, U.K., 1993; Chapt. 4, pp 177−241.
(29) Koppel, D. *J. Chem. Phys.* **1972**, *57*, 4814.
(30) Dobrynin, A.; Colby, R.; Rubinstein, M. *Macromolecules* **1995**, *28*, 1859−1871.
(31) Rigsbee, D. R.; Dubin, P. L. Unpublished results.
(32) Trappe, V.; Weitz, D. *Phys. Rev. Lett.* **2000**, *85* (2), 449−452.
(33) Tadros, T. *Colloids Surf. A: Physicochem. Eng. Aspects* **1994**, *91*, 39.
(34) Leibler, L.; Rubinstein, M.; Colby, R. H. *Macromolecules* **1991**, *24*, 4701.
(35) Lander, A. D. *Matrix Biol.* **1998**, *17*, 465.

BM049174P